STATISTICS, OPTIMIZATION AND INFORMATION COMPUTING
*Stat., Optim. Inf. Comput.*, Vol. **x**, Month 202x, pp 0–15.
Published online in International Academic Press (www.IAPress.org)

# On the Mathematical Modeling of Carotid Bifurcation Stenosis as a Cause of Ischemic Stroke

Arif Fatahillah [1,*], Dzawawi Dimas Adani [1], Robiatul Adawiyah [1], Susi Setiawani [1], Rafiantika Megahnia Prihandini[1], Haci Mehmet Baskonus[2]

[1] *Department of Mathematics Education, Universitas Jember,Indonesia*
[2] *Faculty of Education, Harran University, Sanliurfa, Turkey*

**Abstract** Ischemic stroke is the most common type of stroke, caused by disrupted blood flow to the brain. This study aims to analyze blood flow stenosis in the carotid bifurcation, a major cause of ischemic stroke. A mathematical model is developed using the finite volume method, considering variations in shape, thickness, and stenosis location. The stenosis shapes analyzed include bell-shaped, cosine-shaped, and elliptical, with narrowing levels of 60%, 70%, 80%, and 90%. The mathematical model is solved using the SIMPLE algorithm and simulated in Python to assess the impact of stenosis on ischemic stroke risk. The simulation provides velocity and pressure data across different stenosis shapes and thicknesses, enabling a comprehensive risk analysis. Computational Fluid Dynamics (CFD) is employed to simulate turbulent flow in the carotid bifurcation using ANSYS FLUENT. The findings indicate that 90% stenosis in the carotid bifurcation poses a significant risk, as the resulting flow velocity and pressure exceed normal thresholds. This study provides valuable insights into the effects of carotid bifurcation stenosis on ischemic stroke occurrence and its implications.

**Keywords** Ischemic stroke, Finite volume, Carotid bifurcation

**DOI:** 10.19139/soic-2310-5070-2596

## 1. Introduction

Ischemic stroke is a condition in which brain tissue lacks oxygen and nutrients due to plaque stenosis or blockage in the carotid bifurcation, leading to brain damage [26, 9]. The carotid artery is the only blood vessel that branches into a sinus larger than itself, causing blood flow to become turbulent or irregular in the enlarged sinus area, resulting in cholesterol and calcium plaque more easily accumulating there [21]. This disease is more common in the elderly, although in some countries, healthy individuals have a lower risk [1, 14]. The mortality rate from ischemic stroke in East Asia surpasses that observed in Western countries such as the United Kingdom and the United States [17]. Certain lifestyle habits, including smoking, high cholesterol levels, high fat and high salt diets, hypertension, and lack of exercise, are recognized as factors that increase the risk of ischemic stroke [18, 22].

The stenosis that causes ischemic stroke is primarily due to fatty plaque buildup. The development of fatty plaques tends to occur more frequently in geometrically vulnerable areas, such as the curvature of the carotid bifurcation in the common carotid artery [1, 21]. These plaques typically form an arc-like shape as they develop gradually through the accumulation of cholesterol on the arterial walls. In this study, the investigated stenosis shapes include bell-shaped, cosine-shaped, and elliptical, as they closely resemble real stenosis formations. In addition to the shape variations, stenosis thickness is also varied at 60%, 70%, 80%, and 90%.

Several other studies have focused on stenosis in the carotid bifurcation. Lopez et al. (2021) concluded that blood flow velocity increases while pressure decreases in the stenosed region [10]. Another study by Pinyo et al.

*Correspondence to: Arif Fatahillah (Email: arif.fkip@unej.ac.id). Department of Mathematics Education, Universitas Jember, Jalan Kalimantan 37, 68126, Jember, Jawa Timur, Indonesia

ISSN 2310-5070 (online) ISSN 2311-004X (print)

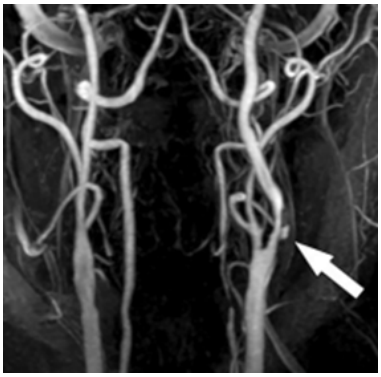

Figure 1. CT Scan of Carotid Bifurcation [15]

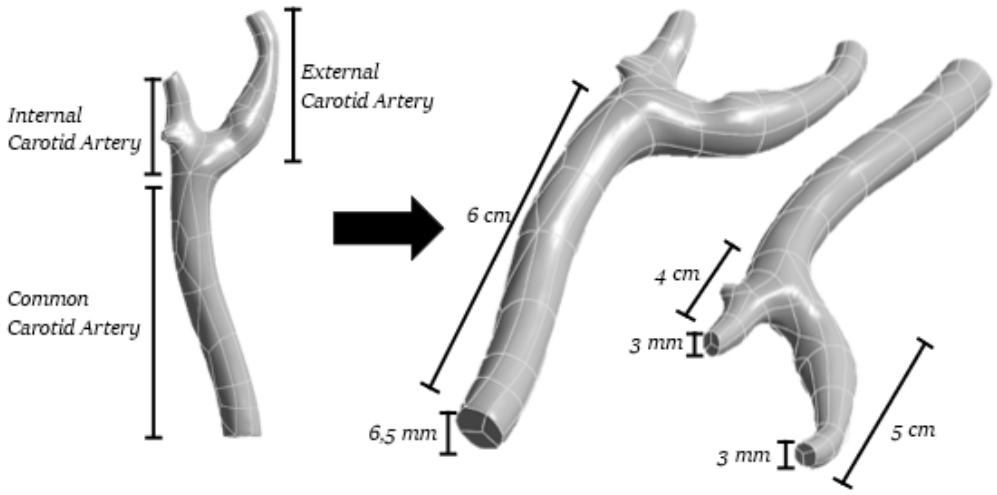


Figure 2. 3D Model of Carotid Bifurcation

(2021) examined a mathematical model of arterial stenosis with bell-shaped and cosine-shaped formations. Their findings also indicated that asymmetric stenosis leads to more complex flow patterns, with more evenly distributed velocity and pressure changes due to the broader distribution of blood flow [20]. The study further revealed that the highest blood flow velocity occurs at the center of the stenosed artery, and the velocity in cosine-shaped stenosis is significantly lower than in bell-shaped stenosis. Meanwhile, Bhavya et al. (2024) focused on elliptical-shaped arterial stenosis caused by radiation and chemical effects. Their research also presented a mathematical model in the form of velocity graphs and contour plots to illustrate the results [8]. The objective of this study is to investigate, in detail, the effects of different stenosis shapes, thicknesses, and locations on blood flow velocity and pressure in the carotid bifurcation, as analyzed through the obtained graphs and contour plots.

## 2. Method

### *2.1. Mathematical Modeling*

Several internal and external factors can contribute to vascular stenosis. This simulation aids medical researchers in understanding the internal factors that influence the narrowing of blood vessel walls. To analyze stenosis and

identify its location, the stenosis shapes are studied, and diagrams are created, as shown in Figure 3. In this simulation, blood is considered a Newtonian fluid with incompressible, unsteady, and turbulent properties.

The fundamental equations governing the boundary conditions for simulating the blood flow hydrodynamics in the carotid bifurcation are defined as follows [16, 4, 25]:

Mass Conservation Equation

$$\nabla \cdot \vec{V} = 0 \tag{1}$$

Momentum Conservation Equation

$$\rho \left( \frac{\partial \vec{V}}{\partial t} + \left( \vec{V} \cdot \nabla \right) \vec{V} \right) = -\nabla p + \mu \nabla^2 \vec{V} \tag{2}$$

Sumit et al. (2023) [24] stated the boundary conditions for the stenosis radius in bell-shaped, cosine-shaped, and elliptical arterial stenosis as follows:

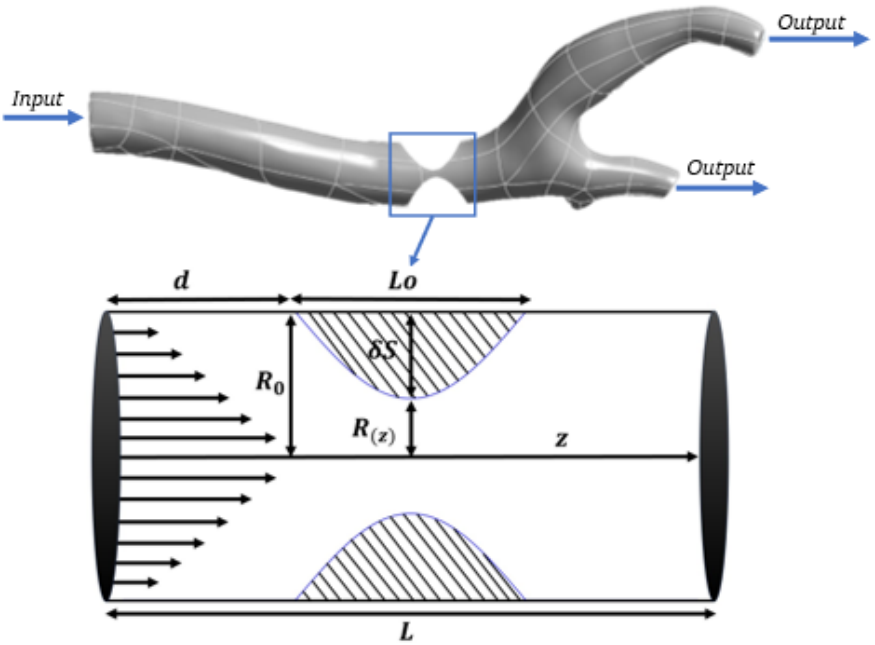


Figure 3. Blood Flow Geometry

Bell-Shaped equation:

$$\begin{cases} R(z) = R_0 - \delta_s e^{\frac{m^2}{R_0^2}\left(z - d - \frac{L_o}{2}\right)^2} & ; d \le z \le d + L_o \\ R(z) = R_0 & ; \text{otherwise.} \end{cases} \tag{3}$$

Cosine-Shaped equation:

$$\begin{cases} R(z) = R_0 - \frac{\delta_s}{2}\left(1 + \cos\frac{2\pi}{L_o}\left(z - d - \frac{L_o}{2}\right)\right) & ; d \le z \le d + L_o \\ R(z) = R_0 & ; \text{otherwise.} \end{cases} \tag{4}$$

Elliptical equation:

$$\begin{cases} R(z) = R_0 - \delta_s \sin\left(\frac{\pi(z-d)}{L_o}\right) & ; d_1 \le z \le d_1 + L_o \\ R(z) = R_0 & ; \text{otherwise.} \end{cases} \tag{5}$$

With:

$R(z)$ = radius on stenosis
$R_0$ = the arterial radius
$\delta_s$ = the maximum height of the stenosis
$L$ = the arterial length
$L_0$ = the total length of the stenosis
$z$ = flow direction
$d$ = stenosis location
$u = v = 0$; at the arterial wall $(r = R(z))$

In the study by Roy et al. (2017), the inlet velocity values are as follows [19]:

$$u = 2U_0 \left(1 - \left(\frac{r}{R(z)}\right)^2\right) \quad ; \text{at the inlet } (x = 0) \tag{6}$$

In Figure 3, R(z) represents the stenosis geometry, which can be mathematically expressed as:

$$R(z) = R_0 \left(1 - \delta e^{-\alpha\left(\frac{x}{R_0}\right)^2}\right) \tag{7}$$

$R_0$ represents the radius of the normal section of the artery, $\delta$ is the maximum height of the stenosis, and $\alpha$ is the stenosis shape parameter.

### *2.2. Discretization*

The mass conservation equation (Equation 2.1) and the momentum conservation equation (Equation 2.2) are used to calculate the velocity and pressure fields in the stenosed carotid bifurcation. The Finite Volume Method (FVM) is applied to discretize these equations [12, 2]. This method is used because it facilitates determining the desired values during the discretization process and has a high level of accuracy suitable for blood flow [7, 10]. To solve the fluid flow equations, the Semi-Implicit Method for Pressure-Linked Equations (SIMPLE) algorithm is employed. This algorithm is widely used in Computational Fluid Dynamics (CFD) to solve fundamental fluid flow equations [13, 3, 5, 6].

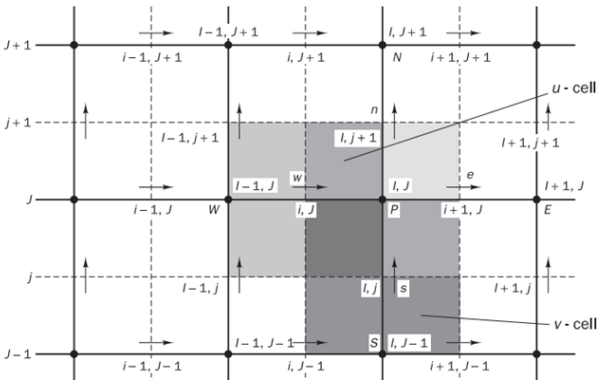


Figure 4. Discretization Scheme of the SIMPLE Algorithm [12]

The steps of the SIMPLE (Semi-Implicit Method for Pressure-Linked Equations) algorithm are as follows: [12, 3]:

1. Initializing Initial Guesses $p^*, u^*, v^*$ dan $\phi^*$.

2. Solving the Discretized Momentum Equations

$$a_{i,j}u^*_{i,j} = \sum a_{nb}u^*_{nb} + \left(p^*_{i-1,j} - p^*_{i,j}\right)A_{i,j} + b_{i,j}$$

$$a_{i,j}u^*_{i,j} = \sum a_{nb}u^*_{nb} + \left(p^*_{i,j-1} - p^*_{i,j}\right)A_{i,j} + b_{i,j}$$

3. Solving the Pressure Correction Equation

$$a_{I,J}p'_{I,J} = a_{I+1,J}p'_{I+1,J} + a_{I-1,J}p'_{I-1,J} + a_{I,J+1}p'_{I,J+1} + a_{I,J-1}p'_{I,J-1} + b'_{I,J}$$

4. Determining the Corrected Pressure and Velocity

$$u'_{i+1,j} = u^*_{i+1,j} + d_{i+1,j}\left(p'_{I,J} - p'_{I+1,J}\right)$$

$$v'_{i,j+1} = v^*_{i,j+1} + d_{I,j+1}\left(p'_{I,J} - p'_{I,J+1}\right)$$

Where,

$$d_{i+1,j} = \frac{A_{i+1,j}}{a_{i+1,j}} \quad \text{and} \quad d_{i,j+1} = \frac{A_{i,j+1}}{a_{i,j+1}}$$

5. Solving All Other Discretized Transport Equations

$$a_{I,J}\phi_{I,J} = a_{I+1,J}\phi_{I+1,J} + a_{I-1,J}\phi_{I-1,J} + a_{I,J+1}\phi_{I,J+1} + a_{I,J-1}\phi_{I,J-1}$$

Check whether the discretized solution has converged. If not, repeat Steps 1–4 until convergence is achieved.

The next step involves discretizing the blood vessel geometry in the carotid bifurcation into a system of linear equations, which will be solved using Python. ANSYS Fluent (version 2024R1, ANSYS Inc.) is used to solve the turbulent flow model of the Newtonian fluid in the carotid bifurcation. This process involves dividing the simulation domain into a set of interconnected small volumes or control cells. The velocity and pressure variables are then computed at the centroids of these cells. ANSYS Fluent employs an iterative algorithm to solve these equations until a converged solution is obtained. The simulation time step size is set to 0.1 seconds, running for 200 iteration steps. The final step is to analyze the simulation results using ANSYS software to derive further conclusions.

### *2.3. Simulation Parameters*

Table 1 presents the factors affecting blood flow rate in the carotid bifurcation due to vascular stenosis [7, 11, 19, 23, 27]. A numerical experiment was conducted to analyze blood flow through a stenotic artery with blockage levels of 60%, 70%, 80%, and 90%.

Table 1. Value of Parameter Factors Affecting Blood Flow Rate

| **Parameter** | **Value** |
|---|---|
| Diameter of *carotid bifurcation* | 6,5 mm |
| Blood Density | 1060 $kg/m^3$ |
| Viscosity | 0,0035 $kg/ms$ |
| Flow Velocity | 0,5 $m/s$ |
| Pressure | 15998.64 $Pa$ |

## 3. Results and Discussion

### *3.1. Results*

The numerical analysis of the carotid bifurcation blood vessel as a cause of ischemic stroke was conducted by analyzing the simulation results from the mathematical model using Python and the geometric design simulation

using Fluent. In Figure 5, for bell-shaped stenosis, blood flow velocity increases with the stenosis percentage. At 45% stenosis, the velocity increase remains moderate (yellow-green area). However, at 90% stenosis, a significant surge in velocity is observed (orange-red area at the stenosis center). The velocity gradient becomes sharper with increased narrowing, raising the risk of arterial wall rupture. In Figure 6, for cosine-shaped stenosis, the diameter transition follows a cosine function pattern. At 60% and 70% stenosis, the maximum velocity is localized at the narrowest point. At 80% and 90% stenosis, a significant velocity spike appears in the central stenosis zone (red area), with a more symmetrical velocity distribution. The velocity gradient becomes sharper, particularly in the peak stenosis region. In Figure 7, for elliptical-shaped stenosis, although the inlet and outlet diameter changes are similar to other shapes, the stenosis peak is more rounded. The flow velocity increases with the stenosis percentage. At 60% and 70% stenosis, the velocity contour pattern is more uniform compared to other stenosis shapes. However, at 80% and 90% stenosis, the peak velocity increases sharply at the narrowest point. This is likely influenced by the elliptical shape, which provides a more stable flow distribution before reaching the maximum stenosis zone.

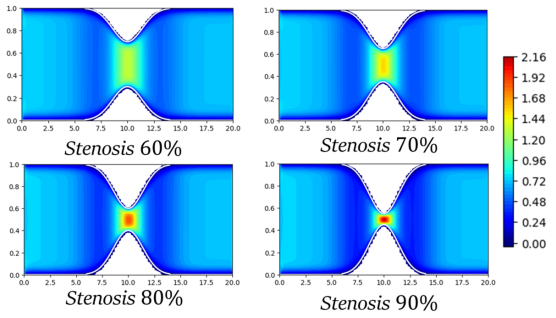


Figure 5. Bell-shaped model with varying stenosis thickness

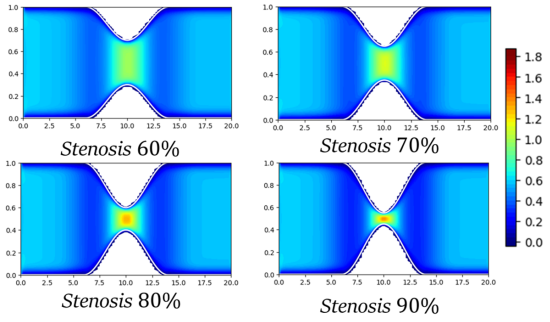


Figure 6. Cosine-shaped model with varying stenosis thickness

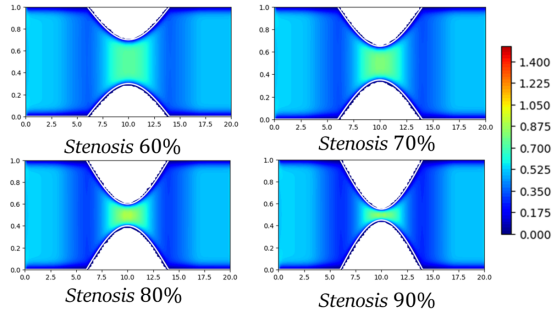


Figure 7. Elliptical model with varying stenosis thickness

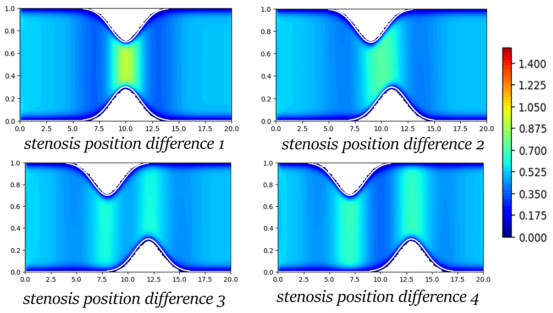


Figure 8. Bell-shaped model with varying stenosis locations

In Figure 8, for the bell-shaped model, the high-velocity region (green-yellow) is concentrated at the stenosis peak, indicating that the fluid flow narrows abruptly. After passing through the stenotic zone, the flow expands again, as shown by the dominance of green-blue colors in the downstream region. In the bell-shaped model, velocity increases based on the stenosis position, with lower velocities at the stenosis site. The further downstream the stenosis is located, the longer the fluid adaptation zone before acceleration at the stenosis point, affecting the flow pattern in the carotid bifurcation. In Figure 9, for the cosine-shaped model, the blue area (low velocity) in the downstream region is more extensive, indicating that flow slows down after passing through the stenosis. The velocity increase in the cosine-shaped model occurs according to the stenosis position, similar to the bell-shaped stenosis. The uniform blue-green contour indicates a more stable velocity distribution due to the variation in stenosis position. In Figure 10, for the elliptical-shaped model, the flow contracts immediately near the stenosis,

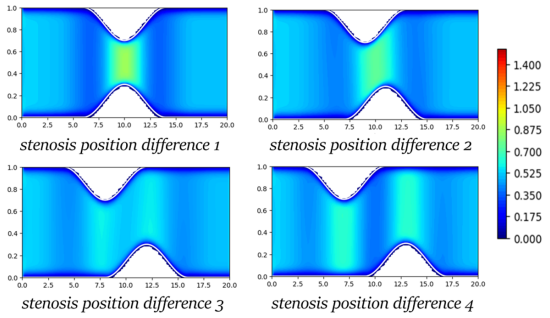


Figure 9. Cosine-shaped model with varying stenosis locations

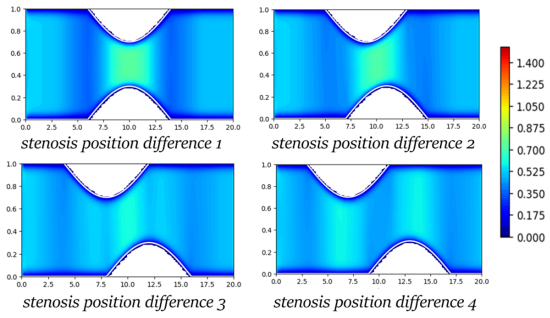


Figure 10. Elliptical model with varying stenosis locations

creating a dominant high-velocity zone (yellow) at the beginning. After the stenotic region, the flow expands and velocity decreases, as shown by the dominance of green-blue colors downstream. In the elliptical model, the maximum velocity shifts according to the stenosis location. The further downstream the stenosis occurs, the longer the adaptation zone before acceleration, influencing the velocity pattern in the carotid bifurcation.

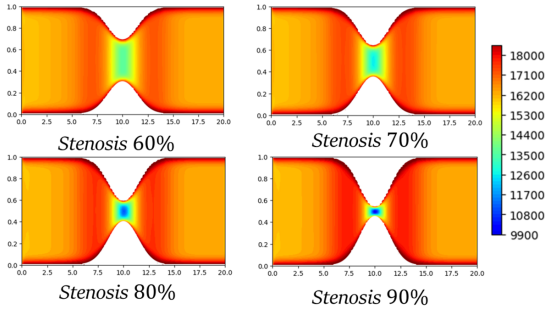


Figure 11. Bell-shaped model with varying stenosis thickness

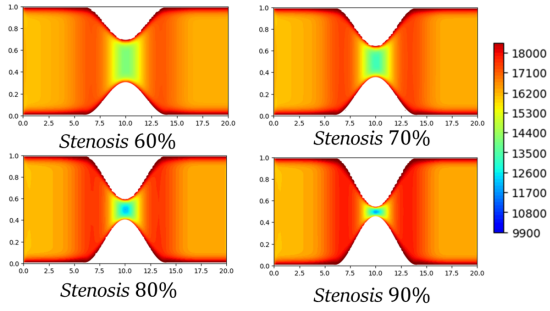


Figure 12. Cosine-shaped model with varying stenosis thickness

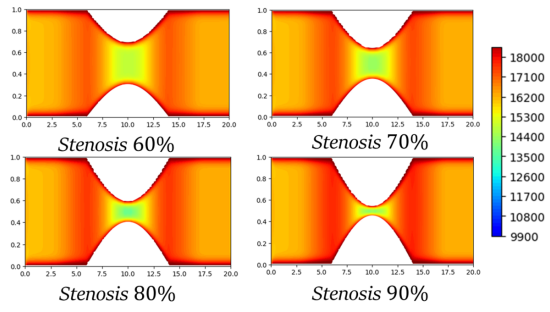


Figure 13. Elliptical model with varying stenosis thickness

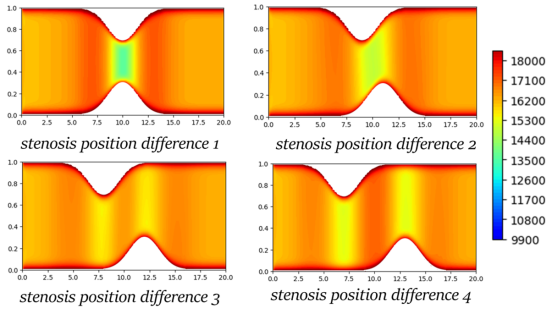


Figure 14. Bell-shaped model with varying stenosis locations

In Figure 11, for the bell-shaped model, at 60% stenosis, the pressure remains uniform with a slight decrease at the narrowest region (light green). At 70% stenosis, the pressure drop becomes more pronounced (yellow-green area). At 80% stenosis, a blue zone begins to appear in the stenotic region, indicating low pressure due to increased velocity. At 90% stenosis, the blue area expands and intensifies, showing the most extreme pressure drop, with a

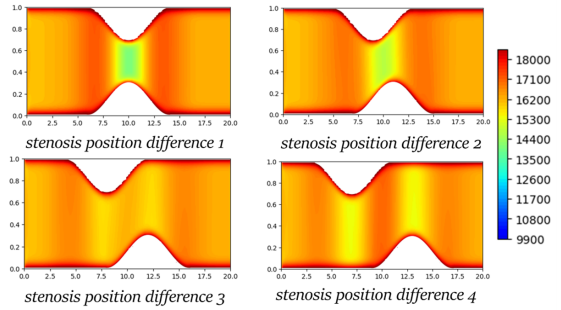


Figure 15. Cosine-shaped model with varying stenosis locations

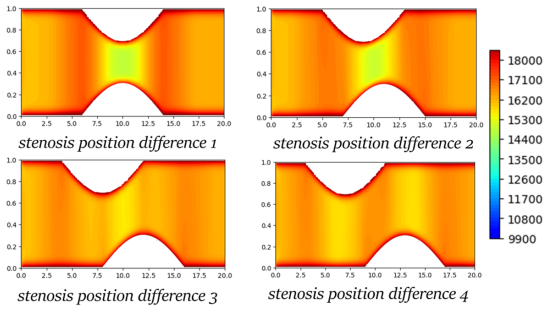


Figure 16. Elliptical model with varying stenosis locations

sharp contrast between the inlet (red) and the stenotic zone (blue). In Figure 12, for the cosine-shaped model, the pressure distribution pattern is similar to that of the bell-shaped stenosis. At 60% stenosis, the pressure remains relatively uniform. At 70% stenosis, the pressure drop in the central region becomes more evident, although the blue zone is not yet dominant. At 80% stenosis, a blue zone appears, indicating low pressure, with a sharp contrast between the inlet (red-orange) and the stenosis region (blue). At 90% stenosis, the blue area intensifies, reflecting a significant pressure drop due to increased flow acceleration. In Figure 13, for the elliptical-shaped model, at 60% stenosis, the pressure drop in the stenotic zone is still minimal (yellow-green area). At 70% stenosis, the pressure drop becomes more noticeable in the central region (green zone). At 80% stenosis, the pressure distribution is almost identical to that of 70% stenosis. At 90% stenosis, the yellow area extends around the stenosis, indicating an increase in velocity and a corresponding pressure drop, though it is less intense compared to the other stenosis shapes.

In Figure 14, the bell-shaped model illustrates the effect of stenosis position on pressure distribution in bell-shaped stenosis. In Position 1, stenosis in the center creates a low-pressure region (yellow-green) around the stenosis peak. In Position 2, the low-pressure area is concentrated in the middle of the channel, with a more uniform pressure gradient. In Position 3, the pressure remains relatively high, dominated by orange-red colors. In Position 4, stenosis at the end of the channel causes high pressure to be more evenly distributed. In Figure 15, the cosine-shaped model shows the impact of stenosis position on flow pressure distribution for cosine-shaped stenosis. In Position 1, stenosis at the center results in low pressure at the stenosis peak. In Position 2, low pressure is concentrated in the middle of the channel, with a more balanced pressure gradient. In Position 3, pressure remains relatively high, with orange-red colors dominating. In Position 4, stenosis at the farthest position leads to a more uniform pressure distribution, maintaining high pressure. In Figure 16, the elliptical-shaped model demonstrates the effect of stenosis position on pressure distribution in elliptical stenosis. In Position 1, with stenosis in the center, low pressure appears at the stenosis peak. In Position 2, the low-pressure area is concentrated in the mid-section of the channel. The pressure gradient remains significant, but is now more evenly distributed due to the smooth transition of the elliptical shape. In Position 3, the pressure contours show a relatively moderate pressure drop, with orange-red zones still dominating. Finally, in Position 4, where stenosis occurs at the farthest location, the pressure remains high, as the pressure induced by stenosis is evenly distributed across the flow.

In Figure 17, the velocity visualization is shown sequentially from left to right for bell-shaped, cosine-shaped, and elliptical stenosis models of blood flow in the carotid bifurcation. For the bell-shaped model, at 60% stenosis, the blue area dominates, indicating low flow velocity. At 70% and 80% stenosis, the green-yellow zones expand around the stenosis, showing a velocity increase. At 90% stenosis, the yellow-red colors are dominant at the narrowest point, indicating a very high velocity. For the cosine-shaped model, the velocity distribution follows a cosine-shaped narrowing pattern. At 60% stenosis, the blue region dominates around the stenosis, representing low velocity. As the stenosis increases to 70% and 80%, green zones appear at the stenosis point, indicating increasing velocity. At 90% stenosis, the yellow-red colors are highly concentrated at the stenosis peak, indicating maximum velocity. For the elliptical-shaped model, at 60% stenosis, the blue color dominance signifies low velocity. At

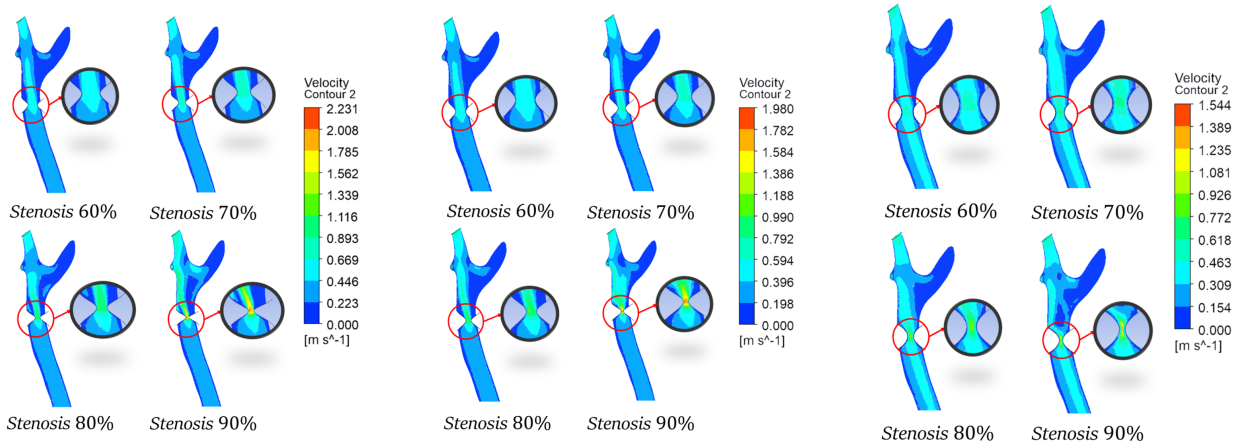


Figure 17. Simulation Results of Velocity in Ansys with Varying Stenosis Thickness

70% stenosis, green zones start appearing, marking a velocity increase. At 80% stenosis, the green-yellow region expands, indicating a significant rise in velocity. At 90% stenosis, the yellow-red zones dominate the narrowest point, showing the highest velocity. Overall, as stenosis severity increases, there is a significant rise in flow velocity at the stenotic region, consistent with the principles of fluid continuity.

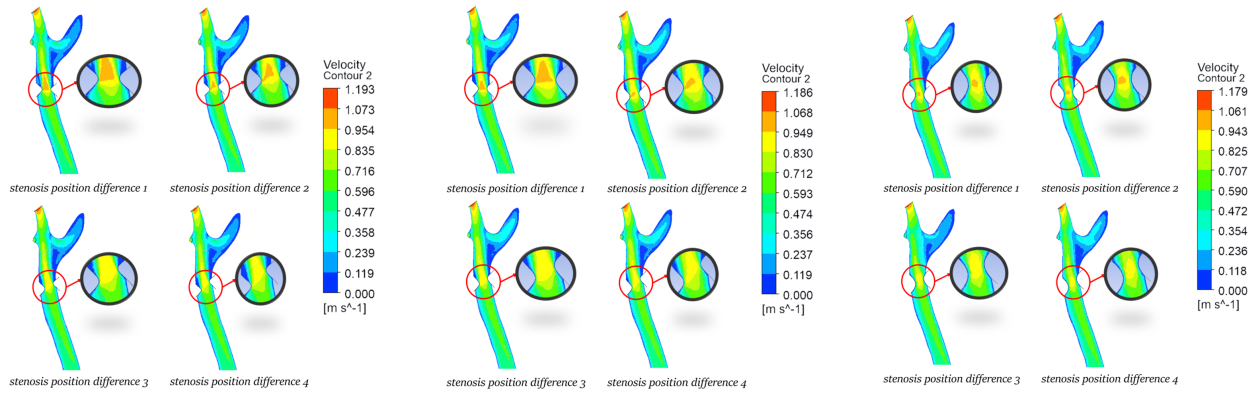


Figure 18. Simulation Results of Velocity in Ansys with Varying Stenosis Locations

In Figure 18, it is shown that the farther the stenosis location, the smaller its impact on velocity increase. This can be observed from Position 1 to Position 4, where the maximum flow velocity tends to decrease due to a more evenly distributed flow. As a result, the acceleration at the stenosis point becomes lower.

In Figure 19, the pressure visualization is shown sequentially from left to right for bell-shaped, cosine-shaped, and elliptical stenosis models of blood flow in the carotid bifurcation. For the bell-shaped model, the visualization includes stenosis levels of 60%, 70%, 80%, and 90%. At 60% stenosis, the pressure remains uniform (predominantly green). At 70% stenosis, the pressure begins to decrease in the stenotic region (dark green). At 80% stenosis, the pressure drops further, approaching blue levels. At 90% stenosis, the minimum pressure is observed, with green-blue colors dominating the narrowest point. As stenosis severity increases, the pre-stenotic pressure rises sharply due to flow resistance, while the pressure at the stenotic region drops significantly. For the cosine-shaped model, the pressure simulation follows a similar pattern. At 60% and 70% stenosis, the pressure remains relatively uniform (green). At 80% stenosis, the pressure drops more significantly, approaching blue levels. At 90% stenosis, the minimum pressure is observed, with green-blue colors dominating the stenotic region. For the elliptical-shaped

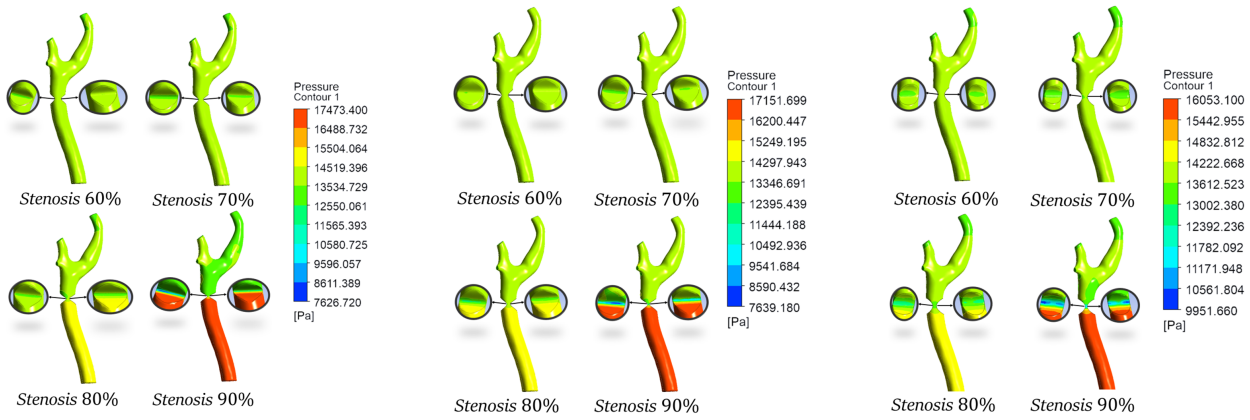


Figure 19. Simulation Results of Pressure in Ansys with Varying Stenosis Thickness

model, the pressure simulation shows that at 60% stenosis, the pressure remains uniform (green). At 70% stenosis, the pressure begins to decrease (dark green). At 80% stenosis, the pressure further declines, nearing blue levels. At 90% stenosis, the minimum pressure is dominant at the narrowest point (green-blue). All simulations demonstrate that increasing stenosis severity leads to a sharp rise in pre-stenotic pressure, while the pressure at the stenotic region decreases due to flow acceleration.

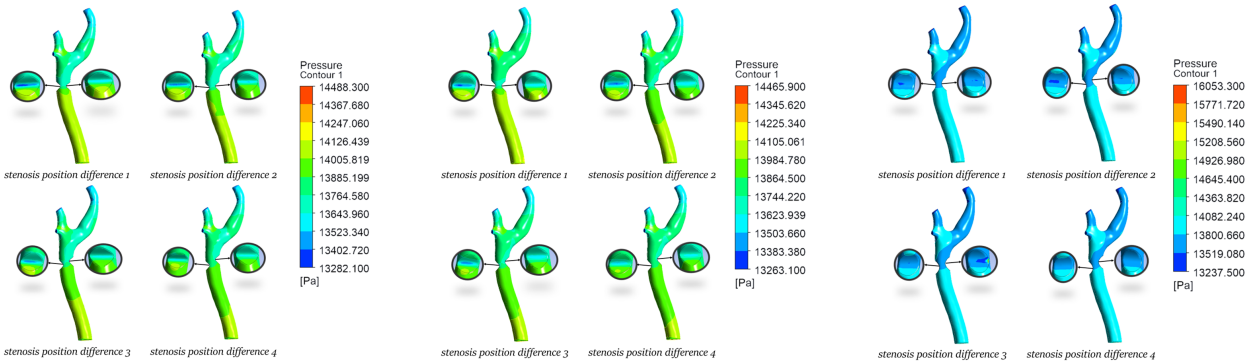


Figure 20. Simulation Results of Pressure in Ansys with Varying Stenosis Locations

In Figure 20, it is shown that the farther the stenosis location, the smaller its impact on pressure reduction. From Position 1 to Position 4, the pressure drop is not significant. Different stenosis positions result in a more uniform pressure distribution, leading to higher overall pressure compared to symmetrical stenosis with the same cross-sectional area.

Figure 21 illustrates the wall shear stress (WSS) distribution at different levels of stenosis severity (60%–90%). It is evident that as the degree of narrowing increases, the maximum WSS values tend to rise and become more concentrated around the most constricted regions. These high-WSS areas may impose significant mechanical stress on the arterial wall, potentially contributing to plaque instability and increasing the risk of rupture.

### *3.2. Discussion*

The graphs in Figures 22 to 27 present the simulation results using Python and Fluent, considering different stenosis thicknesses in the carotid bifurcation. These graphs indicate that before reaching the stenotic region, the blood pressure tends to be high, then gradually decreases towards the stenosis center. Conversely, the flow velocity is

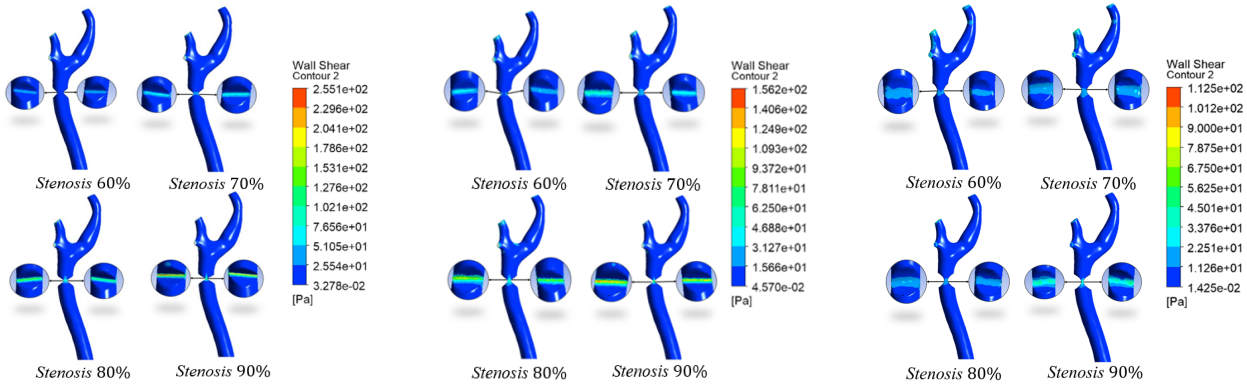


Figure 21. The simulation results of wall shear stress (WSS)

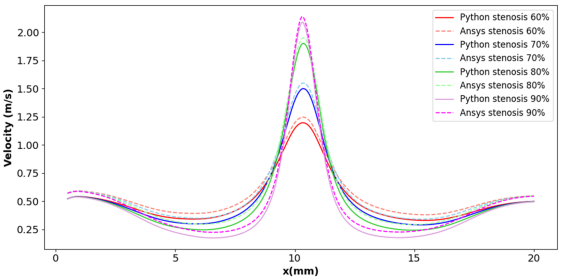


Figure 22. Velocity graph of a bell-shaped model with varying stenosis thickness

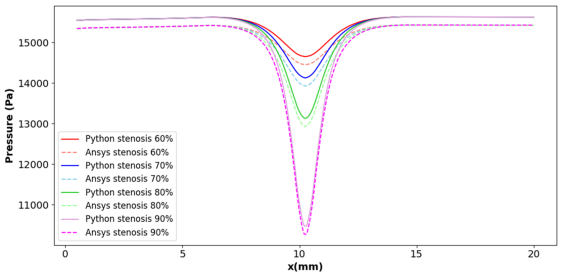


Figure 23. Pressure graph of a bell-shaped model with varying stenosis thickness

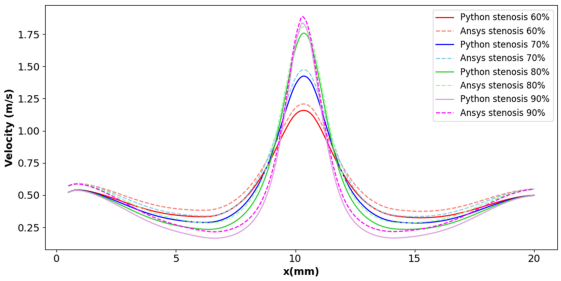


Figure 24. Velocity graph of a cosine-shaped model with varying stenosis thickness

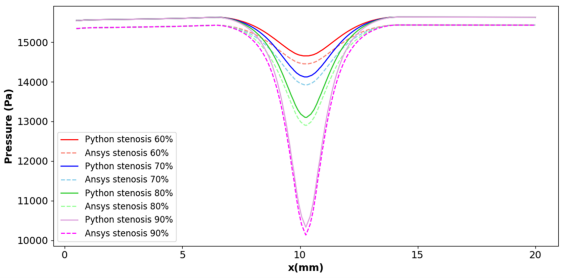


Figure 25. Pressure graph of a cosine-shaped model with varying stenosis thickness

initially low but increases as it approaches the stenotic center. Beyond the stenotic region, pressure rises again as the flow cross-sectional area increases, while velocity decreases. These findings align with the study by Lopez et al. [10], which reported that blood pressure before stenosis tends to be high and subsequently drops toward the stenosis center, while flow velocity increases in the narrowing region and has the same flow pattern and stenosis effect as the study by S. Kumar et al 2023 [24]. Furthermore, the data reveal that among the three stenosis models analyzed (bell-shaped, cosine-shaped, and elliptical), the bell-shaped model has the most significant impact on velocity and pressure changes. These results support the findings of Pinyo et al. (2021) and Bhavya et al. [8, 20], which stated that the bell-shaped stenosis leads to a more significant velocity increase and a sharper pressure drop in the stenotic region compared to other shapes.

To ensure that the numerical simulation results are independent of mesh size or element count, a grid independence study was conducted by comparing the peak velocity and peak pressure drop across three mesh

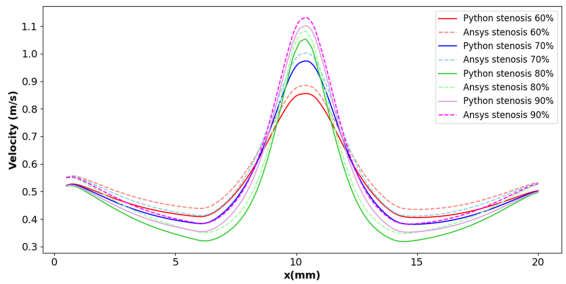


Figure 26. Velocity graph of a elliptical model with varying stenosis thickness

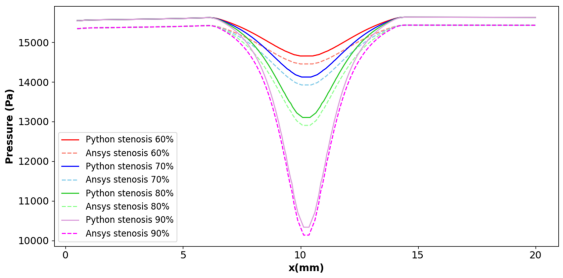


Figure 27. Pressure graph of a elliptical model with varying stenosis thickness

Table 2. Comparison of Peak Velocity and Peak Pressure for Bell-Shaped Stenosis at Different Mesh Sizes.

| **Mesh Size** | **Number of Nodes** | **Peak Velocity** | | **%Difference** | **Peak Pressure Drop** | | **%Difference** |
|---|---|---|---|---|---|---|---|
| | | **MATLAB** | **ANSYS** | | **MATLAB** | **ANSYS** | |
| Coarse Mesh | 75702 | 2.076 | 2.231 | 7.19% | 9820.138 | 10420.14 | 5.92% |
| Medium Mesh | 163891 | 2.054 | 2.160 | 5.03% | 9880.15 | 10220.12 | 3.38% |
| Fine Mesh | 309720 | 2.048 | 2.089 | 1.98% | 9910.23 | 10017.91 | 1.08% |

Table 3. Comparison of Peak Velocity and Peak Pressure for Cosine-Shaped Stenosis at Different Mesh Sizes.

| **Mesh Size** | **Number of Nodes** | **Peak Velocity** | | **%Difference** | **Peak Pressure Drop** | | **%Difference** |
|---|---|---|---|---|---|---|---|
| | | **MATLAB** | **ANSYS** | | **MATLAB** | **ANSYS** | |
| Coarse Mesh | 75702 | 1.697 | 1.802 | 6.00% | 10526.12 | 10989.341 | 4.30% |
| Medium Mesh | 163891 | 1.721 | 1.787 | 3.76% | 10646.172 | 10889.282 | 2.25% |
| Fine Mesh | 309720 | 1.741 | 1.767 | 1.48% | 10734.784 | 10878,142 | 1.32% |

Table 4. Comparison of Peak Velocity and Peak Pressure for Elliptical Stenosis at Different Mesh Sizes.

| **Mesh Size** | **Number of Nodes** | **Peak Velocity** | | **%Difference** | **Peak Pressure Drop** | | **%Difference** |
|---|---|---|---|---|---|---|---|
| | | **MATLAB** | **ANSYS** | | **MATLAB** | **ANSYS** | |
| Coarse Mesh | 75702 | 0.987 | 1.048 | 5.99% | 13372.132 | 14140.563 | 5.58% |
| Medium Mesh | 163891 | 0.988 | 1.024 | 3.57% | 13433.113 | 13940.593 | 3.70% |
| Fine Mesh | 309720 | 0.991 | 1.005 | 1.40% | 13197.137 | 13640.165 | 1.05% |

resolutions: coarse, medium, and fine. The comparison results are presented in Tables 2 through 4 for different stenosis shapes. It can be observed that the percentage differences between MATLAB and ANSYS results decrease as the mesh becomes finer, indicating that the solution has achieved numerical convergence. Therefore, the fine mesh was selected for the final simulations to ensure solution accuracy and stability.

Figure 28 presents a comparison of blood flow velocity profiles along the axial direction (z) for three scenarios: normal condition (red solid line), initial velocity variation (blue dashed line), and fluid density variation (green dotted line). These results indicate that the study has taken into account the uncertainty arising from variations in input parameters such as velocity and density, which can affect the hemodynamic simulation outcomes. Although

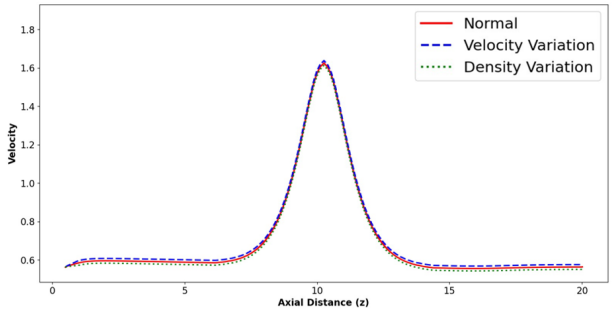


Figure 28. Comparison of Blood Flow Velocity Profiles for Three Scenarios

slight differences are observed, the overall flow pattern remains consistent, suggesting that the model's validity is maintained within the range of parameter variations analyzed.

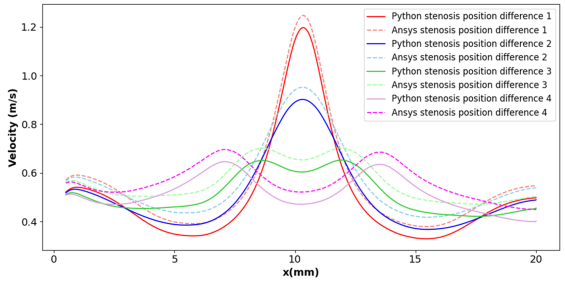


Figure 29. Velocity graph of a bell-shaped model with varying stenosis location

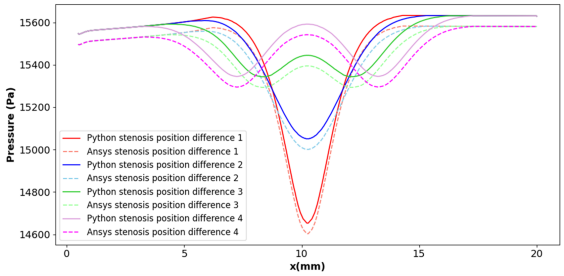


Figure 30. Pressure graph of a bell-shaped model with varying stenosis location

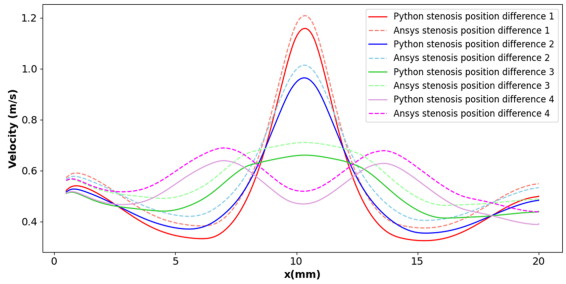


Figure 31. Velocity graph of a cosine-shaped model with varying stenosis location

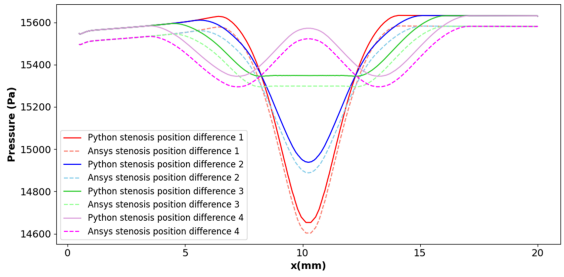


Figure 32. Pressure graph of a cosine-shaped model with varying stenosis location

Figures 28 to 33 present simulation graphs obtained using Python and Fluent, aimed at observing the effect of different stenosis locations on fluid flow dynamics. The simulation results indicate that the farther the stenosis is from the initial position, the lesser its impact on flow velocity increase. This occurs because as the stenosis shifts away from the initial position, the fluid flow becomes more evenly distributed, causing the maximum velocity to decrease compared to stenosis located closer to the initial position. This velocity reduction can be explained by a more uniform flow distribution, where the fluid's kinetic energy is spread over a larger area. In contrast, in cases of thicker and more symmetrical stenosis, the fluid flow tends to concentrate in a specific region, resulting in a more significant velocity increase. These findings align with the study conducted by Pinyo et al. (2021) [20], which

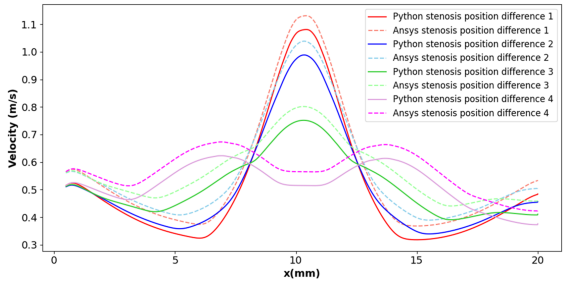


Figure 33. Velocity graph of a elliptical model with varying stenosis location

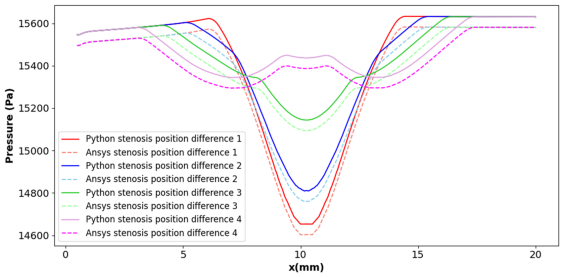


Figure 34. Pressure graph of a elliptical model with varying stenosis location

stated that in asymmetric stenosis, the flow pattern becomes more complex, with more evenly distributed velocity and pressure changes due to wider flow dispersion.

Table 5. Flow Velocity and Pressure Data for the Three Shape Models

| **Shape of Stenosis** | **Thickness Level (%)** | **Velocity (m/s) / Pressure (Pa)** |
|---|---|---|
| *Bell-shaped* | 60% | 1 – 1,2 / 14300 – 15200 |
| | 70% | 1,4 – 1,6 / 13400 – 14300 |
| | 80% | 1,8 – 2 / 11600 – 13400 |
| | 90% | 2 – 2,1 / 9800 – 10700 |
| *Cosine-shaped* | 60% | 1 – 1,1 / 14300 – 15200 |
| | 70% | 1,1 – 1,2 / 13400 – 14300 |
| | 80% | 1,3 – 1,6 / 12000 – 14000 |
| | 90% | 1,6 – 1,8 / 10000 – 11000 |
| *Elliptical* | 60% | 0,525 – 0,7 / 14300 – 15200 |
| | 70% | 0,7 – 0,85 / 13400 – 14300 |
| | 80% | 0,85 – 0,9 / 13400 – 14400 |
| | 90% | 0,85 – 1,050 / 13200 – 14200 |

Figure 35 illustrates the temporal evolution of plaque growth in the carotid artery over a period of 5, 10, and 15 years. It can be observed that over time, the degree of arterial lumen narrowing increases due to progressive plaque accumulation. This is indicated by the intensifying red zone, representing higher blood flow velocity in the stenotic area as the narrowing becomes more severe. This reflects increasingly complex hemodynamic dynamics as the disease progresses.

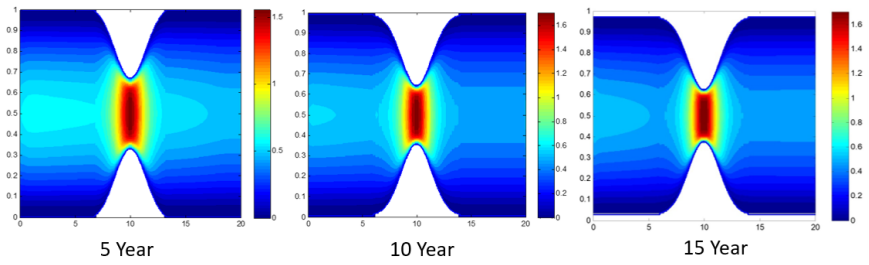


Figure 35. Evolution of Stenosis Growth

Thus, it can be concluded that thicker and more symmetrical stenosis tends to have a greater impact on the increase in flow velocity compared to stenosis that shifts away from the initial position. Additionally, the simulation results indicate that the stenosis location significantly influences the pressure distribution within the fluid flow. As the stenosis moves farther from the initial position, its effect on pressure reduction becomes less significant. This relatively small pressure drop occurs because the pressure within the fluid flow is more evenly distributed, preventing a sharp decrease in specific areas. In contrast, in cases of thicker and more symmetrical stenosis, the pressure drop is more pronounced, as the fluid flow is concentrated at a specific point, leading to a more uneven pressure distribution.

From this analysis, it can be concluded that thicker and more symmetrical stenosis leads to a greater increase in flow velocity and a more significant pressure drop, accompanied by high wall shear stress (WSS) that can cause damage to blood vessels, compared to stenosis with different shapes or positions. This indicates that the shape and location of the stenosis have a significant influence on fluid flow characteristics and the increased potential for plaque formation.

## 4. Conclusion

This study has simulated the effect of stenosis in the carotid bifurcation in the context of ischemic stroke and analyzed how it influences blood flow characteristics. Additionally, this study has validated a mathematical model of blood flow in the carotid bifurcation for bell-shaped, cosine-shaped, and elliptical stenosis with varying degrees of narrowing, ranging from 60% to 90%. The key findings of this study are as follows:

- Numerical simulations and CFD results indicate that 90% stenosis in all stenosis shapes within the carotid bifurcation is highly dangerous, potentially leading to arterial rupture.
- Flow velocity and pressure drop increase gradually as stenosis thickness increases, emphasizing the importance of early intervention—the sooner stenosis is detected and treated, the better the chances of preventing severe complications.
- Asymmetrical stenosis placement reduces its impact on velocity and pressure due to the more evenly distributed flow, resulting in less localized pressure buildup.

## Acknowledgement

This research is supported by the Computational Research Group and Virtual Laboratory, Department of Mathematics Education, University of Jember, Jember, Indonesia

REFERENCES

1. Ali Müftüoğulları and Münir Süner and Buğra Sarper The effect of bifurcation angulation on flow characteristics and hemodynamic indicators in an idealized left coronary artery. *International Journal of Thermofluids* 2024. P. 100554. 10.1016/j.ijft.2023.100554
2. Anley, E. F. Numerical Solutions of Elliptic Partial Differential Equations by Using Finite Volume Method. *Pure and Applied Mathematics Journal* 2016. Vol. 5. 10.11648/J.PAMJ.20160504.16
3. Arif Fatahillah, Basuki Widodo, Rozaini Roslan Mathematical modeling of Ischaemic central retinal vein occlusion using finite volume method. *AIP Conf. Proc.* 2024. 10.1063/5.0222460
4. A Fatahillah, B Widodo, R Roslan The Modeling and Numerical Solution of Branch Retinal Artery Occlusion. *Malaysian Journal of Mathematical Sciences* 2025. Vol. 19 10.47836/mjms.19.1.01
5. Arif Fatahillah, Dimas Agung Prasetyo, Robiatul Adawiyah, Susi Setiawani, Arika Indah Kristiana Numerical modelling of blood vessel constriction due to peripheral artery disease using finite volume method. *AIP Conf. Proc.* 2024. 10.1063/5.0222462
6. Attar, H., Ahmed, T., Rabie, R., Amer, A., Khosravi, M. R., Solyman, A., & Deif, M. A. Modeling and computational fluid dynamics simulation of blood flow behavior based on MRI and CT for Atherosclerosis in Carotid Artery. *Multimedia Tools and Applications* 2024. Vol. 83. 10.1007/s11042-023-17765-w
7. A. Ostadfar Chapter 1 - Fluid Mechanics and Biofluids Principles. *Academic Press* 2016. P. 1–60. 10.1016/B978-0-12-802408-9.00001-6
8. B. Tripathi and B. K. Sharma Two-phase analysis of blood flow through a stenosed artery with the effects of chemical reaction and radiation. *Ricerche mat* 2024. Vol. 73 P. 151–177. 10.1007/s11587-021-00571-7

9. Costa D, Scalise E, Ielapi N, Bracale UM, Faga T, Michael A, Andreucci M, Serra R. Omics Science and Social Aspects in Detecting Biomarkers for Diagnosis, Risk Prediction, and Outcomes of Carotid Stenosis. *Biomolecules* 2024. Vol. 8 10.3390/biom14080972
10. D. Lopes and R. Agujetas and H. Puga and J. Teixeira and R. Lima and J.P. Alejo and C. Ferrera Analysis of finite element and finite volume methods for fluid-structure interaction simulation of blood flow in a real stenosed artery. *International Journal of Mechanical Sciences* 2021. Vol. 207 P. 106650. 10.1016/j.ijmecsci.2021.106650
11. E. Nader et al. Blood Rheology: Key Parameters, Impact on Blood Flow, Role in Sickle Cell Disease and Effects of Exercise. *Front. Physiol* 2019. Vol. 10 P. 1329. 10.3389/fphys.2019.01329
12. H. K. Versteeg and W. Malalasekera An Introduction to Computational Fluid Dynamics: The Finite Volume Method. *New York: Wiley* 2007.
13. H. Khawaja and M. Moatamedi Semi-implicit method for pressure-linked equations (SIMPLE) solution in MATLAB. *Int. J. Multiphys* 2018. Vol. 12 P. 313. 10.21152/1750-9548.12.4.313
14. J. L. M. Björkegren and A. J. Lusis Atherosclerosis: Recent developments. *Cell* 2022. Vol. 185 P. 1630–1645. 10.1016/j.cell.2022.04.004
15. L. Saba et al. State-of-the-art CT and MR imaging and assessment of atherosclerotic carotid artery disease: the reporting—a consensus document by the European Society of Cardiovascular Radiology (ESCR). *Eur. Radiol* 2023. Vol. 33 P. 1088–1101. 10.1007/s00330-022-09025-6
16. M. A. Hamidah and S. M. C. Hossain CModeling analysis of pulsatile non-Newtonian blood flow in a renal bifurcated artery with stenosis. *Int. J. Thermofluids* 2024. Vol. 22 P. 100645. 10.1016/j.ijft.2024.100645
17. M. Lou et al. Chinese Stroke Association guidelines for clinical management of cerebrovascular disorders: executive summary and 2019 update on organizational stroke management. *Stroke Vasc. Neurol* 2020. Vol. 5 10.1136/svn-2020-000355
18. M. Malvè, G. Finet, M. Lagache, R. Coppel, R. I. Pettigrew, and J. Ohayon Chapter 10 - Hemodynamic disturbance due to serial stenosis in human coronary bifurcations: a computational fluid dynamics study. *Academic Press* 2021. Vol. 4 P. 225–250. 10.1016/B978-0-12-817195-0.00010-X
19. M. Roy, B. Singh Sikarwar, M. Bhandwal, and P. Ranjan Modelling of Blood Flow in Stenosed Arteries. *Procedia Comput. Sci* 2017. Vol. 115 P. 821–830. 10.1016/j.procs.2017.09.164
20. P. Owasit and S. Sriyab Mathematical modeling of non-Newtonian fluid in arterial blood flow through various stenoses. *Adv. Differ. Equations* 2021. Vol. 1 P. 340. 10.1186/s13662-021-03492-9
21. Pelz DM, Fox AJ, Spence JD, Lownie SP Carotid Stenosis and Stroke: Historical Perspectives Leading to Current Challenges. *Canadian Journal of Neurological Sciences / Journal Canadien des Sciences Neurologiques* 2025. Vol. 52. 10.1017/cjn.2024.40
22. Robert J. Henning, Brian L. Hoh The diagnosis and treatment of asymptomatic and symptomatic patients with carotid artery stenosis. *Current Problems in Cardiology* 2025. Vol. 50 10.1016/j.cpcardiol.2025.102992.
23. S.-K. Jeong and R. S. Rosenson Shear rate specific blood viscosity and shear stress of carotid artery duplex ultrasonography in patients with lacunar infarction. *BMC Neurol* 2013. Vol. 13 P. 36. 10.1186/1471-2377-13-36
24. S. Kumar and S. Kumar Blood Flow with Heat Transfer through Different Geometries of Stenotic Arteries. *Trends Sci* 2023. Vol. 20 P. 6965. 10.48048/tis.2023.6965
25. Ul Haq, U., Ahmed, A., Mustansar, Z., Shaukat, A., Cukovic, S., Nadeem, F., ... Margetts, L. Computational modeling and simulation of stenosis of the cerebral aqueduct due to brain tumor. *Engineering Applications of Computational Fluid Mechanics* 2022. Vol. 16 P. 1018–1030. 10.1080/19942060.2022.2056511
26. W.-J. Tu et al. Estimated Burden of Stroke in China in 2020. *JAMA Netw. open* 2023. Vol. 6 10.1001/jamanetworkopen.2023.1455
27. W. Meng et al. Concentration Polarization of High-Density Lipoprotein and Its Relation with Shear Stress in an In Vitro Model. *J. Biomed. Biotechnol* 2009. P. 695838 10.1155/2009/695838